Journal of Magnetics 31(2), 240-249 (2026)

ISSN (Print) 1226-1750
ISSN (Online) 2233-6656
https://doi.org/10.4283/JMAG.2026.31.2.240

# Innovative Antenna Design for IoT Sensing Systems in Smart Agriculture

**Ahmed Laiche[1]*, Hamza Ben Hamadi[1,2], Said Ghnimi[1], Mohamed Salah Karoui[1,3], and Ali Gharsallah[1]**

[1]*Laboratory of Microwave Electronics, Faculty of Sciences of Tunis, University of Tunis El Manar, Tunis, Tunisia*
[2]*Universite Clermont Auvergne, EUPI, CNRS, Institut Pascal, F-63000 Clermont-Ferrand, France*
[3]*Higher Institute of Applied Sciences and Technology of Mateur, University of Carthage, Tunisia*

(Received 20 January 2026, Received in final form 16 May 2026, Accepted 18 May 2026)

**This paper investigates the design, simulation, and experimental validation of an innovative omnidirectional microstrip patch antenna array operating at 2.45 GHz for agricultural Internet of Things (IoT) applications. Addressing the limitations of conventional directional and MIMO antenna systems particularly in terms of coverage, cost, and environmental adaptability, the proposed design integrates a Wilkinson power divider network and employs a compact dual-element configuration with curved slots to enhance impedance matching and radiation characteristics. The antenna is fabricated on an FR-4 substrate and optimized using full-wave electromagnetic simulations. Experimental validation conducted in a real agricultural nursery demonstrates reliable data acquisition from distributed sensor nodes irrespective of their spatial orientation. Furthermore, the measured results exhibit strong agreement with simulation predictions in terms of reflection coefficient, gain, and electromagnetic field distribution. These findings confirm the suitability of the proposed antenna array as a robust, low-cost solution for wireless sensor communication in smart farming environments.**

**Keywords :** antenna array, microstrip patch antenna, radiation efficiency, Wi-Fi application, wireless communications

## 1. Introduction

The growing emphasis on precision agriculture and environmental monitoring has, in recent years, driven researchers to explore the development of efficient and reliable wireless communication solutions tailored for agricultural applications [1, 2]. Among these, WiFi-based solutions operating at 2.45 GHz have attracted considerable attention due to their balance between connectivity range and data transmission performance [3]. Several studies have emphasized the importance of designing antennas with adequate gain, directional stability, and environmental robustness to ensure seamless operation in outdoor agricultural conditions [4, 5]. To meet these requirements, the Wilkinson power divider-based antennas have been explored as a promising approach [6, 7]. These structures are known for their excellent impedance matching, high isolation between output ports, and ability to produce balanced radiation suitable for wide-area coverage [8]. Recent implementations of Wilkinson antennas have demonstrated gains in the range of 5–8 dBi, making them suitable for moderate-range agricultural deployments [9]. Moreover, as highlighted in [10], the integration of such antennas with microcontroller systems particularly Arduino-based platforms has expanded their capabilities, enabling real-time data acquisition, processing, and wireless transmission. These integrated systems are especially attractive for large-scale sensor networks monitoring key parameters such as soil moisture, humidity, and ambient temperature [11]. The low power consumption of Arduino microcontrollers further supports the viability of these solutions in battery- or solar-powered scenarios commonly found in remote agricultural settings [12].

Additionally, researchers have proposed several enhancements to Wilkinson feeding networks to optimize bandwidth, efficiency, and radiation pattern stability in variable field conditions [4]. Recent efforts have concentrated on improving the design for real-world deployment by addressing challenges such as weather resistance, cost, and mechanical flexibility [13]. In this context, the use of conformal substrates has also been explored [14], making it possible to integrate antennas directly onto farming equipment or structural surfaces. These advancements have significantly promoted the use of 2.45 GHz Wilkinson


*Corresponding author: Tel: +216-58-828-350
Fax: +216-71-871-666, e-mail: ahmed.laiche@fst.utm.tn

antenna arrays for diverse smart farming applications, including automation and environmental monitoring [15]. With these efforts, a critical review of the existing literature reveals persistent limitations in currently deployed antenna solutions for agricultural IoT. where unidirectional designs, such as those employing λ/4 transformer feed networks, require precise physical alignment with sensor nodes and are unsuitable for randomly deployed wireless sensor networks [17, 21]. MIMO-based systems offer improved channel capacity but introduce substantial design complexity and cost that are prohibitive in low-power, cost-sensitive field deployments [5, 16]. Large-array configurations (8–16 elements) achieve high gain [18, 19] but at the expense of prohibitively large physical footprints incompatible with portable or mounted agricultural equipment. Conformal arrays on flexible substrates have been demonstrated [20], yet none of the reported designs combine compactness, omnidirectionality, and real-world agricultural validation simultaneously. To overcome these constraints, the present work proposes a novel dual-element microstrip patch antenna array fed by a Wilkinson power divider network. The Wilkinson topology was specifically selected for its well-established ability to provide equal power splitting, excellent inter-port isolation, and superior impedance matching—all critical to maintaining radiation pattern uniformity when feeding multiple radiating elements [6, 7]. Unlike MIMO-based solutions which, despite their performance benefits, entail significantly higher cost and design complexity the proposed approach offers a cost-effective, compact, and easily fabricated alternative on the widely available FR-4 substrate [16]. The principal novelty and contributions of this work are threefold: (1) the design of the smallest reported Wilkinson-based dual-element patch array on FR-4 at 2.45 GHz, occupying only 41.5 × 36.5 mm$^2$; (2) the introduction of optimized curved-slot elements that simultaneously achieve a deep return loss of −41 dB and a wide operating bandwidth spanning 2.15–3.43 GHz; and (3) a comprehensive real-world experimental validation performed in a functioning agricultural nursery, confirming the system's reliability in a practical IoT precision farming deployment. The proposed antenna demonstrates enhanced omnidirectional coverage, improved gain, and robust radiation characteristics, making it a viable and practical solution for modern smart farming wireless sensor networks.

The manuscript is organized as follows. Section 2 examines Precision Agriculture technologies and describes the antenna development process through a comprehensive parametric analysis of these applications. Section 3 presents both computational modeling results and experimental findings for the patch antenna array incorporating a Wilkinson power divider. Finally, Section 4 summarizes the results and provides recommendations for future research.

## 2. Materials and Methods

Agricultural IoT devices are attracting growing interest across the precision farming sector. This section presents the deployment context of the proposed system within a real agricultural nursery, describes the key connected objects and sensing infrastructure, and details how smart wireless technologies contribute to improved monitoring of farm conditions. In this work, our objective is to implement a base station connected to an Arduino system for remote monitoring. The installation is deployed in a small agricultural nursery equipped with several wireless sensors. Each sensor collects environmental data such as soil moisture and temperature (Fig. 1).

These technologies result from four distinct actions: the first, data collection using smart agricultural sensors. These smart sensors can collect information about the growth of your plants. They include a wireless communication module to allow data to be sent to applications.

The second, connectivity, allows the data collected by

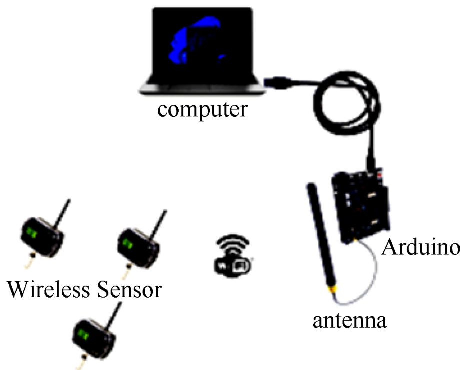


**Fig. 1.** (Color online) Conceptual Diagram of the Wireless Sensor Network Architecture.

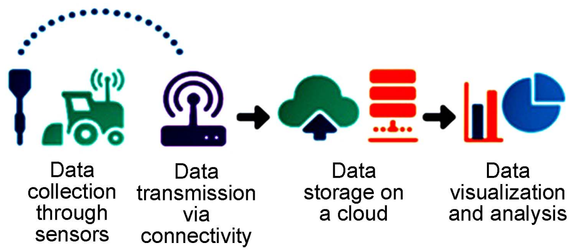


**Fig. 2.** (Color online) Technologies and the Internet of Things (IoT) in Smart Agriculture.

the sensors to be sent to a cloud that will store the information directly online. The Wi-Fi module facilitates the transmission of this information. The third is data storage, which is sent via the communication network and received on your cloud or on the cloud of your IoT provider. They are at this point raw; it is time to use decision support technologies. The last phase is the visualization and interpretation of the collected data (Fig. 2).

It is at this stage that the collected information will be analyzed and various decision-making technologies come into play. Using raw data and various algorithms, this raw information will be transformed into dashboards, graphs, recommendations, etc., becoming true allies in your decision-making.

In this context, our work focuses on the connectivity phase, which plays a crucial role in precision agriculture technologies. The Wi-Fi antenna's radiation performance and compatibility with wireless sensor networks must be key design aspects, ensuring robust data reception over a wide area.

Initially, our investigation focused on analyzing currently deployed wireless antennas utilized within radio frequency communication systems and their implementation across diverse domains including Internet of Things applications and agricultural sectors. Our work focuses specifically on agricultural applications, aiming to improve wireless monitoring of environmental conditions in nurseries.

In this work, an omnidirectional antenna was designed for precision agriculture and related applications. It can be interfaced with an Arduino Mega board via a Wi-Fi module to enable wireless data transmission. The design aims to enhance radiation characteristics and improve gain, thereby optimizing the coverage area. This wide coverage allows reliable signal reception from sensor nodes distributed throughout the nursery without requiring precise alignment. The proposed antenna, intended for Wi-Fi applications at a resonance frequency of 2.45 GHz, was designed using the High-Frequency Structure Simulator (HFSS). It was fabricated on an FR-4 substrate with a relative permittivity of 4.3, a dielectric loss tangent of 0.025, and a thickness of 1.6 mm. A microstrip transmission line was used for feeding, as illustrated in Fig. 3.

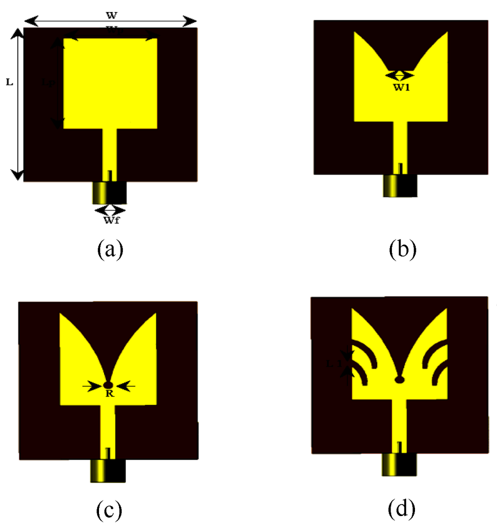


**Fig. 3.** (Color online) Evolution of the proposed antenna 1 design: (a) initial rectangular patch, (b) introduction of slots, (c) circular slot modification, and (d) final antenna with curved slots for enhanced performance.

The configuration initiates with a fundamental rectangular patch antenna element (a) that functions as the primary structural foundation. During phase (b), triangular apertures are incorporated along the upper boundaries to augment impedance coordination and frequency response characteristics. Following this, in stage (c), a centrally positioned circular aperture is integrated to refine the emission characteristics and enhance current flow optimization.

Ultimately, configuration (d) features the integration of curved apertures positioned on either side of the central circular aperture, which serves to optimize the radiating element's electromagnetic performance, enhance directional gain, and establish superior all-directional field coverage appropriate for wireless transmission systems deployed in farming applications (Table 1).

To further elaborate on the theoretical modeling of the antenna, the following section presents the key equations and concepts used to characterize the radiation and impedance behavior of a rectangular microstrip patch antenna:

The analysis assumes that the electric field distribution remains uniform across the patch width W. The radiation

**Table 1.** Dimensions of the proposed antenna.

| Parameter | Dimensions (mm) |
|---|---|
| W | 36.5 |
| L | 41.5 |
| Wf | 4 |
| Wp | 19.88 |
| Lp | 24.52 |
| R | 1.9 |
| W1 | 4 |
| L1 | 1.34 |
| Hs | 1.6 |
| Ht | 0.035 |

characteristics of a single slot can then be described as follows. The radiation susceptance of an individual slot is given by:

$$B = \frac{2\pi \Delta L \sqrt{\varepsilon_{eff}}}{\lambda_0 Z_0} \tag{1}$$

where:

$$Z_0 = \frac{120\pi h}{W\sqrt{\varepsilon_{eff}}} \tag{2}$$

$$f_r = \frac{c}{2\sqrt{\varepsilon_{eff}}(L + 2\Delta l)} \tag{3}$$

Here, $\lambda_0$ denotes the free-space wavelength, and $Z_0$ is the characteristic impedance of the microstrip line, which is defined based on its length L and width W.

The effects of the surrounding medium and the electric field distribution at the substrate's ends are captured using the effective relative dielectric constant, defined in Eq. (4):

$$\varepsilon_{eff} = \frac{\varepsilon_r + 1}{2} + \frac{\varepsilon_r - 1}{2}(1 + 12\frac{h}{W})^{-\frac{1}{2}} \tag{4}$$

The edge extension, commonly known as the effective length extension, is given by:

$$\frac{\Delta L}{h} = 0.412h\frac{(\varepsilon_{eff} + 0.3)(\frac{W}{h} + 0.264)}{(\varepsilon_{eff} - 0.258)(\frac{W}{h} + 0.8)} \tag{5}$$

To determine the antenna impedance, the slot admittance is combined with transmission line theory. The operating frequency, which depends on the substrate's dimensions, is expressed by:

$$f_r = \frac{c}{2\sqrt{\varepsilon_{eff}}(L + 2\Delta l)} \tag{6}$$

The input admittance is then calculated using the corresponding dimensions of the radiating edge and the slot's location.

Based on the theoretical framework provided by Eqs. (1-6), the reflection coefficient $S_{11}$ of the proposed antenna is expressed as:

$$S_{11} = \frac{Y_{in}Z_0 - 1}{Y_{in}Z_0 + 1} \tag{7}$$

The antenna's bandwidth is defined by:

$$BW(\%) = 100\frac{f_{\max} - f_{\min}}{f_r} \tag{8}$$

The frequency, $f_{\max}$ and fmin correspond to the frequency limits at a specified reflection level (typically -10 dB). The effective dielectric constant and edge extension equations are applied alongside the cavity model to compute the resonant frequency $f_r$ of rectangular patch antennas.

The resonant mode frequency $f_{mn}$ of a rectangular patch with height h, width W, and length L is approximately given by:

$$f_{mn} = \frac{c_0}{2\sqrt{\varepsilon_{eff}}}\sqrt{\left[\left(\frac{m}{L_e}\right)^2 + \left(\frac{n}{W_e}\right)^2\right]} \tag{9}$$

where m and n are integers (with m = 1 and n = 0 for the dominant mode), and $L_e$ and $W_e$ represent the effective length and width, respectively.

These effective dimensions are approximated by:

$$L_e = L + 2\Delta L \qquad W_e \approx W \tag{10}$$

In this model, all antenna dimensions (specifically L and W) are considered as part of a primary cavity supporting a surface current distribution.

The proposed modification was implemented using the HFSS simulator, a robust full-wave electromagnetic tool used for modeling, simulating, and analyzing the electrical and radiative characteristics of the antenna design.

In the initial rectangular patch configuration (Step A), radiation originates predominantly from the two radiating edges parallel to the E-field direction, where the fringing fields at the open-circuit boundaries extend beyond the physical patch periphery and radiate into free space. The resonant frequency and radiation resistance at these apertures are governed by the effective dielectric constant and the extended effective length of the patch, as expressed in Eqs. (4)–(6). When triangular slots are introduced along the upper edges in Step B, the effective electrical length of the surface current path is increased without enlarging the physical footprint, thereby lowering the resonant frequency and improving impedance matching by reducing the quality factor of the cavity. The subsequent integration of the central circular aperture in Step C further perturbs the current distribution by introducing a localized region of reduced current density at the patch center, which modifies the mutual admittance between the two radiating edges and shifts the resonance toward the target 2.45 GHz band while simultaneously

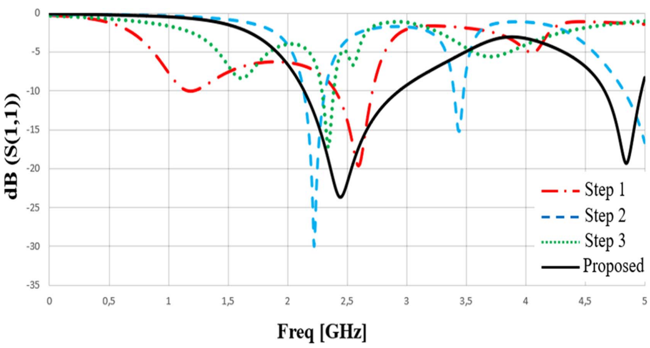


**Fig. 4.** (Color online) Simulated return loss $S_{11}$ comparison across design evolution stages of the proposed antenna 1.

broadening the impedance bandwidth. In the final configuration (Step D), the symmetrically placed curved slots on either side of the central circular aperture introduce two near-degenerate resonant modes with slightly different effective path lengths. The constructive superposition of these two modes gives rise to the observed dual-resonance behavior in Fig. 4 (resonances at 2.45 GHz and 4.8 GHz) and the substantially extended bandwidth (2.15–3.43 GHz).

Figure 4 illustrates the variation of the $S_{11}$ return loss parameter with frequency for the designed microstrip patch antenna configurations.

The simulated reflection coefficient ($S_{11}$) values for the antenna design are illustrated in Fig. 4, demonstrating the progressive development from the initial design phase (Step 1) through intermediate modifications (Step 3) to the ultimate proposed antenna structure. The return loss improves progressively with each modification. In Step 1, the antenna exhibits a minimum $S_{11}$ of -20 dB at 2.66 GHz. In Step 2, the introduction of additional slots enhances the impedance matching, resulting in a deeper notch at 2.25 GHz with an $S_{11}$ of -30 dB. Step 3 further refines the bandwidth and return loss, reaching -17 dB at 2.36 GHz. The Proposed design achieves the best performance, with two distinct resonant frequencies respectively at 2.45 GHz and 4.8 GHz, and corresponding return losses of -24 dB et -19 dB, indicating dual-band behavior suitable for Wi-Fi and related applications.

**Table 2.** Characteristics of the proposed antenna 1.

| Parameter | Value |
|---|---|
| Gain (dB) | 2.58 |
| Bandwidth (GHz) | 1.8–3.5 |
| Directivity (dBi) | 2.96 |
| Efficiency (%) | 87 |
| Impedance Matching | VSWR ≈1,15 |

Table 2 summarizes the main characteristics of the antenna under study. The listed parameters provide key insights into the antenna's performance in terms of signal propagation and reception capabilities. In particular, the authors highlight the antenna's gain, frequency response range, radiation pattern directivity, power conversion efficiency, and impedance matching characteristics.

The results obtained are satisfactory and fall within the expected range for a typical antenna operating in the Wi-Fi band, generally around 2.4 GHz. The gain is sufficient to ensure good coverage, the bandwidth effectively spans the required frequency range, and the directivity is appropriate for use in typical indoor or professional environments. The efficiency is acceptable, ensuring minimal power loss, and the impedance matching is well achieved, allowing for efficient signal transmission with minimal reflection.

Although the single-element microstrip antenna demonstrates satisfactory performance in terms of gain and radiation coverage, it remains limited when broader spatial coverage and enhanced signal strength are required, particularly in complex environments such as agricultural fields. To address these limitations, our study progresses toward a two-element antenna configuration based on a Wilkinson power divider (Fig. 5). This methodology enables enhanced power allocation across the system, superior impedance coordination, and diminished electromagnetic interference among the antenna elements. By integrating a Wilkinson network, we aim to significantly enhance the gain and uniformity of the radiation pattern, thereby achieving a more robust and omnidirectional coverage.

A conventional two-way Wilkinson power divider consists of two quarter-wavelength (λ/4) transmission lines connecting the input port to the two output ports. The characteristic impedance Z_arm of each transmission line branch is given by Eq. (11), where $Z_0$ is the system reference impedance (typically 50 Ω). An isolation resistor R is placed between the two output ports to absorb any reflected power and improve inter-port isolation. For

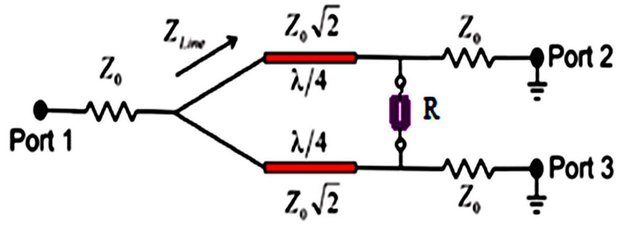


**Fig. 5.** (Color online) Equivalent circuit model for the calculation of the return loss $S_{11}$.

equal power division, R = $2Z_0$ = 100 Ω.

$$Z_{\text{line}} = Z_0\sqrt{2}\,\frac{Z_0 + j\sqrt{2}Z_0\tan(\theta)}{\sqrt{2}Z_0 + jZ_0\tan(\theta)} \tag{11}$$

$$\theta = \frac{2\pi}{\lambda}\cdot\frac{\lambda_0}{4} = \frac{\pi}{2} \tag{12}$$

Where $Z_0$ is the system reference impedance (typically 50 Ω). These lines connect the input port to the two output ports. Additionally, a resistor $R = 2Z_0$ is placed between the two output ports to absorb the power from any reflected signal, thereby improving isolation.

The input impedance looking into both arms of the proposed patch antenna array integrated with a Wilkinson power divider is expressed as:

$$Z_{\text{in}} = \frac{Z_{\text{line}}}{2} \tag{13}$$

The theoretical analysis is performed using even–odd mode decomposition. For equal power division, the reflection coefficient $S_{11}$ can be derived as follows:

$$S_{11} = \frac{Z_{\text{in}} - Z_0}{Z_{\text{in}} + Z_0} \tag{14}$$

In this paper, a two-way Wilkinson power divider is integrated to feed a dual-element patch antenna array operating at 2.45 GHz. The antenna system is fabricated on an FR-4 substrate with a dielectric constant $\varepsilon_r = 4.3$ and a thickness $h = 1.6$ mm. For optimal impedance matching, all ports are designed for $Z_0 = 50$ Ω. Given the lossy nature of FR-4 at 2.45 GHz, meticulous EM simulation and physical layout optimization are required to minimize dielectric and conductor losses, which are more significant compared to low-loss substrates like Rogers or Duroid.

The power divider ensures that both radiating elements receive equal power, crucial for maintaining omnidirectional radiation. Furthermore, the isolation resistor reduces mutual coupling between the patches, preserving the uniformity of the radiation pattern, as confirmed by the measured Sparameters and radiation characteristics. This design choice facilitates robust communication with sensor nodes deployed irregularly in agricultural fields, ensuring consistent signal reception in all azimuth directions an essential requirement for IoT-based smart agriculture applications.

This proposed design, shown in Fig. 6, not only strengthens the antenna's ability to maintain reliable communication with distributed sensor nodes but also

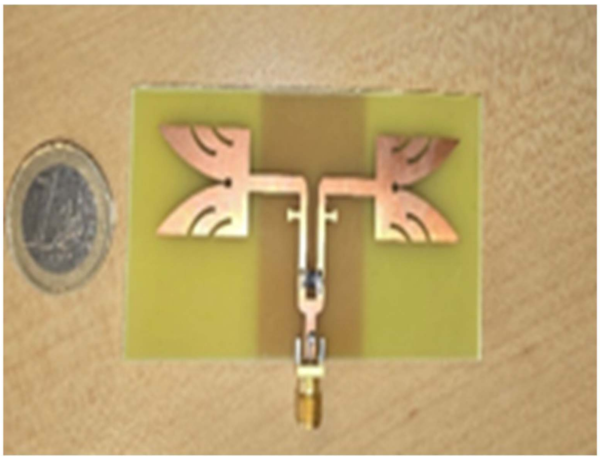

**Fig. 6.** (Color online) Real antenna 2 integrated with a Wilkinson power divider.

aligns with the design requirements for scalable and efficient wireless systems in smart farming applications.

Figures 6 and 7 present the fabricated and measured prototype of the Wilkinson power divider-based omnidirectional antenna designed for Wi-Fi applications at 2.45 GHz. The structure consists of two symmetrically arranged radiating elements connected through a microstrip Wilkinson power divider network. The incorporation of curved slots in the patch elements improves impedance matching and enhances omnidirectional radiation characteristics. A surface-mounted resistor is used to ensure isolation between the output ports, thereby reducing mutual coupling and signal reflection. The compact form factor of the proposed antenna facilitates its integration into IoT-enabled agricultural monitoring systems. Fig. 8 presents the measured and simulated return loss ($S_{11}$) of the proposed antenna as a function of frequency.

Figure 8 demonstrates excellent concordance between

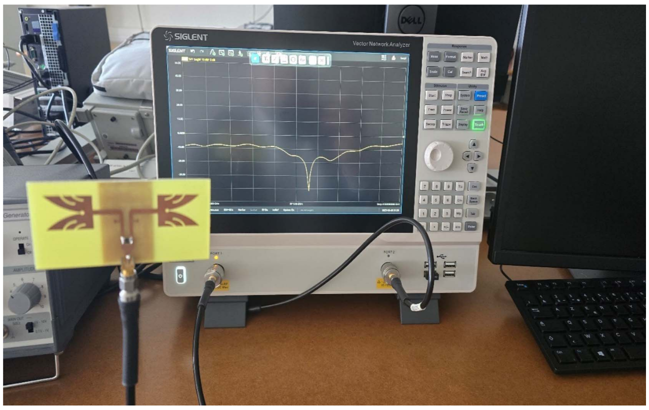


**Fig. 7.** (Color online) The step of measured of $S_{11}$ parameter of the proposed antenna 2.

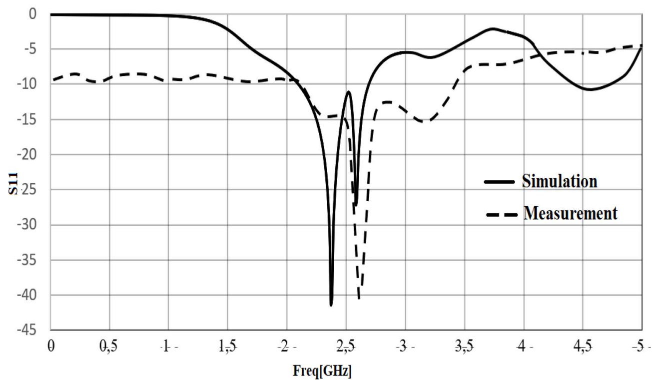


**Fig. 8.** Comparison of Simulated and Measured return loss $S_{11}$ of the proposed antenna 2.

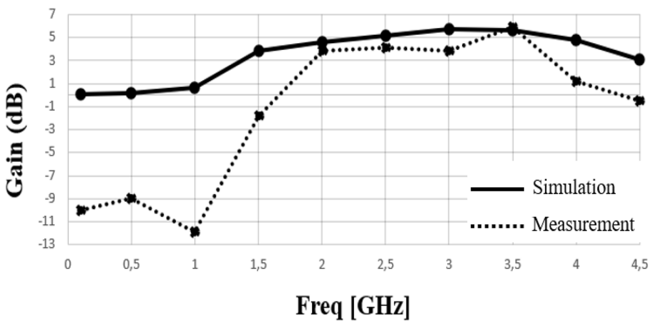


**Fig. 9.** Comparison of Simulated and Measured Gain of the proposed antenna 2.

both curves in the vicinity of the 2.45 GHz resonance frequency, at which point the return loss attains -41 dB, thereby signifying optimal impedance matching performance. The antenna demonstrates broad operational frequency range coverage extending from 2.15 GHz to 3.43 GHz, validating its appropriateness for 2.45 GHz Wi-Fi implementation. Minor discrepancies between the curves are attributed to fabrication and simulation tolerances uncertainties. This discrepancy can be explained by production inconsistencies, material variability, or testing parameters (including cables, connectors, and environmental factors) that were not incorporated into the computational model. As for the $S_{11}$ amplitude, the difference may result from additional losses in the real prototype (dielectric losses, conduction losses, poor contacts). This comparison highlights the importance of integrating real-world parameters into models to improve simulation fidelity.

A comparative analysis of the simulated versus experimental gain measurements for the developed antenna design is presented in Fig. 9, encompassing frequencies from 0.1 GHz to 4.5 GHz.

The radiation mechanism of the proposed antenna can be rigorously interpreted through classical microstrip cavity model theory and fringe field analysis applied to each design stage. The peak directional gains of 4.56 dBi and 3.2 dBi in the E- and H-planes respectively are consistent with the radiation efficiency of 87 % and the compact two-element aperture size, as corroborated by the close agreement between simulated and measured gain curves in Fig. 9.

The antenna demonstrates a significant enhancement in gain as frequency increases, achieving its highest performance at approximately 2.45 GHz where the simulated gain reaches a maximum value of 4.17 dB. The measured curve follows a similar trend, albeit with some deviations due to fabrication imperfections, environmental influences,

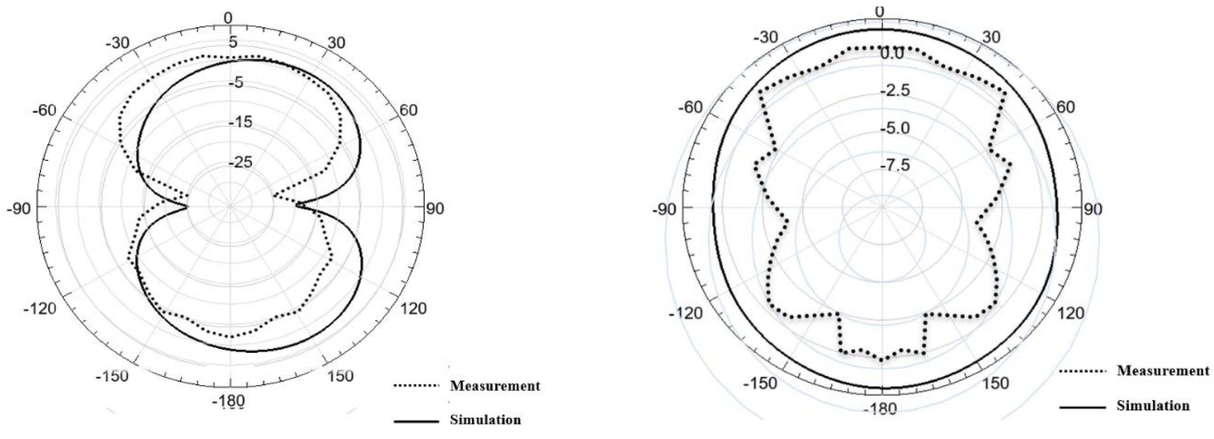


(a)    (b)

**Fig. 10.** Radiation Pattern of the proposed Antenna 2 (a) E-plane (b) H-plane.

and measurement uncertainties. Despite these differences, both results confirm the antenna's operational suitability for Wi-Fi applications around 2.45 GHz, making it a viable solution for wireless data transmission in precision agriculture and related fields.

Furthermore, the geometric symmetry of the curved slots ensures that the current distribution remains balanced about the feed axis, which is the physical condition responsible for the stable, low-cross-polarization omnidirectional pattern in the H-plane confirmed by the measured radiation patterns in Fig. 10.

The radiation characteristics of antenna 2, both computationally modeled and experimentally obtained, are presented in Fig. 10 for operation at 2.45 GHz frequency. Subfigure (a) presents the E-plane ($\varphi = 0°$) radiation characteristics, while subfigure (b) shows the H-plane ($\varphi = 90°$) response.

The experimental data and computational results demonstrate strong concordance, validating the antenna's multidirectional radiation characteristics and broad angular range. Small discrepancies observed between experimental data and computational predictions may result from manufacturing variations and ambient conditions present throughout the measurement process. The antenna maintains stable radiation in both principal planes, indicating its suitability for wireless sensor networks in precision agriculture. The peak directional gains observed in the E- and H-planes reach values of roughly 4.56 dBi and 3.2 dBi, respectively, confirming the antenna's efficient operational characteristics for practical implementation scenarios. These characteristics validate the antenna's suitability for wireless sensor networks in agricultural environments, ensuring reliable communication.

## 3. Results and Discussion

The performance of the fabricated omnidirectional antenna was evaluated through multiple experimental trials conducted in a real agricultural greenhouse facility (referred to as the "nursery"). Several wireless sensor nodes were deployed throughout the facility, including two soil moisture sensors and two temperature sensors, each equipped with compact antennas for data transmission to a central base station. The experiments involved placing the sensor nodes at different locations relative to the base station. The nodes were positioned not only in front of the antenna but also behind it and at various angular orientations, as illustrated in the following Fig. 11.

The results demonstrated that the base station, equipped with our Wilkinson-based omnidirectional antenna, successfully received data from all sensor nodes regardless of their orientation or position. This confirmed the wide radiation pattern and high gain of our antenna, allowing it to capture signals over a large spatial coverage area. Unlike traditional directional antennas, which require precise alignment to communicate effectively, our antenna provided reliable data collection even when the sensor nodes were placed behind or at oblique angles relative to the base station. These findings validate the effectiveness of our design in agricultural IoT applications, where sensor nodes may be distributed irregularly (Fig. 11).

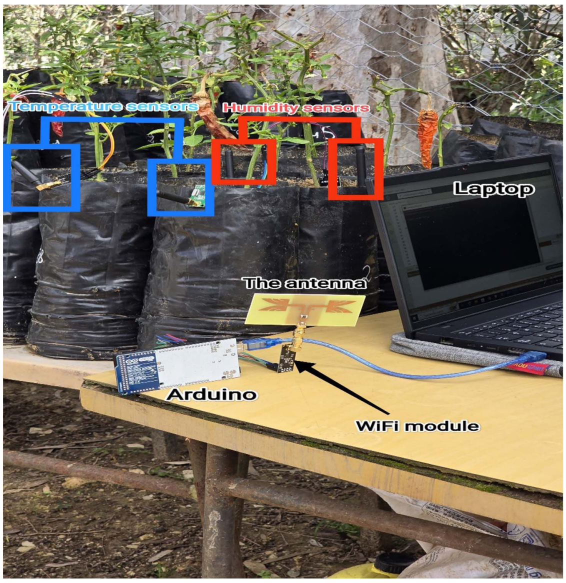

**Fig. 11.** (Color online) Experimental setup in agricultural nursery using omnidirectional Antenna with Sensor Nodes.

To empirically validate the performance of the proposed antenna 2 system within a real-world agricultural setting, we conducted a series of field measurements using wireless sensor nodes using Platform for IoT deployed throughout a nursery environment (Fig. 11). These nodes were equipped with temperature and soil moisture sensors, transmitting data wirelessly to a central base station outfitted with the omnidirectional antenna. The purpose of this practical experiment was to evaluate the system's data acquisition capabilities in a dynamic, outdoor context. The following table presents a representative sample of data collected during this experiment, highlighting the time-stamped readings from the deployed sensors.

Table 3 summarizes the sensor readings collected over a 270-second field testing interval. The dataset includes time-series measurements from two temperature sensors and two soil moisture sensors deployed at fixed locations

**Table 3.** Sensor Data Collected During Field Testing of the Wireless Sensor Network.

| Time (s) | Temperature Sensor 1 (°C) | Temperature Sensor 2 (°C) | Soil Moisture Sensor 1 (%) | Soil Moisture Sensor 2 (%) |
|---|---|---|---|---|
| 0 | 26 | 26 | 42 | 39 |
| 30 | 27 | 27 | 44 | 40 |
| 60 | 25 | 24 | 41 | 41 |
| 90 | 26 | 25 | 43 | 42 |
| 120 | 27 | 26 | 40 | 43 |
| 150 | 25 | 27 | 42 | 38 |
| 180 | 26 | 24 | 44 | 39 |
| 210 | 27 | 25 | 41 | 40 |
| 240 | 25 | 26 | 43 | 41 |
| 270 | 26 | 27 | 40 | 42 |

within the test nursery. As shown, the temperature sensors recorded stable values ranging from 24 °C to 27 °C, while the soil moisture readings exhibited slight variations attributable to the heterogeneous soil composition and non-uniform moisture distribution.

The consistent reception of data across all time steps affirms the antenna's ability to maintain robust communication with sensor nodes regardless of their spatial orientation. This observation supports the effectiveness of the omnidirectional radiation pattern in achieving comprehensive coverage in practical smart agriculture applications.

Table 4 provides a comprehensive comparative analysis of our proposed architecture against multiple structural designs that have been recently reported in the scholarly literature, thereby demonstrating the significance of our research contribution within the current academic discourse.

The Table 4 highlights a clear comparison between various array antennas available in the literature and the one proposed in this work. It emerges that our antenna clearly stands out for its compactness, simplicity of design, and suitability for modern agricultural applications.

Indeed, with only two radiating elements and very small dimensions (41.5 × 36.5 mm²), it occupies the smallest surface area of all the solutions compared, while maintaining a wide bandwidth (2.15–3.43 GHz) compatible with wireless communication systems dedicated to smart agriculture (WiFi, LoRa, ISM, etc.). Its gain of 4.56 dBi, although moderate compared to some larger phased array systems, remains perfectly sufficient to ensure stable connectivity over large agricultural areas, particularly thanks to its quasi-omnidirectional radiation pattern.

Furthermore, the use of the inexpensive and widely available FR-4 substrate, combined with a conformal structure (flexible or adaptable to non-planar surfaces), makes this antenna particularly suitable for integration into field-deployed sensors, drones, or mobile agricultural equipment.

Based on the findings of this study, it can be concluded that the proposed design achieves an effective balance between performance, cost, size, and flexibility, making it well suited for the requirements of connected agriculture and field monitoring systems.

**Table 4.** Comparison of the proposed structure with some references.

| Ref | Feed technique | Size in mm$^2$ | Element of the array | Bandwidth in GHz | Gain | Substrate | Conformal |
|---|---|---|---|---|---|---|---|
| [17] | λ/4 transformer line | 139×76, 271×92, 127×32 | 5, 9, 9 | 2.24–3.0, 5.6–7.2, 5.6–7.2 | 10.6, 13.7, 10.6 | FR-4 | no |
| [18] | WPD | - | 16 | 8.5–11.5 | 13.7 | Rogers 4003 | no |
| [19] | WPD | 900×730 | 16 | 1.25–1.45 | 16.4 | FR-4, NELCO | no |
| [20] | λ/4 transformer line | 800×92 | 8 | 6–16 | 19 | polyamide | Yes |
| [21] | λ/4 transformer line | 120×78.7 | 4 | 3–10.65 | 12.3 | Taconic TLY-5A | no |
| [22] | WPD, Phase shifter | 130×80 | 4 | 2.2–11.6 | 11.5 | FR4, Rogers 4003 | no |
| [23] | Corporate feed | 53.2×53.2 | 2 | 2.4 | 5.67 | FR-4 | no |
| [24] | Microstrip line (indirect) | 123×65 | 2 | 2.3–2.5 | 7.63 | FR-4 | no |
| This wok | WPD | 41.5×36.5 | 2 | 2.15–3.43 | 4.56 | FR-4 | Yes |

## 4. Conclusions

This work validates a multidirectional microstrip patch antenna with a Wilkinson power divider for 2.45 GHz agricultural IoT applications. The design achieves improved impedance matching, gain, and radiation uniformity, with experimental results closely matching simulations and confirming reliable communication in real-world conditions. Its compact, low-cost structure overcomes key limitations of conventional antennas, while offering scalability to larger arrays and adaptability to other frequency bands, making it suitable for efficient and extensible smart farming systems.

Furthermore, the antenna dimensions can be readily rescaled to operate at other frequency bands relevant to smart agriculture, such as 868 MHz (LoRaWAN), 915 MHz (ISM), and 5.8 GHz (Wi-Fi), using standard microstrip design equations. These features make the proposed antenna a flexible and extensible solution for robust environmental monitoring systems.

## References


[1] T. Miller, G. Mikiciuk, I. Durlik, M. Mikiciuk, A. Łobodzińska, and M. Śnieg, Sensors **25**, 3583 (2025).
[2] J. A. Brenes and G. Marín-Raventós, in Intelligent Sustainable Systems, Lecture Notes in Networks and Systems 333, Springer Nature, Singapore (2022) pp. 103~112.
[3] S. Havriliuc, A. Lavric, A. I. Petrariu, E. Coca, and V. Popa, in Proc. 2024 Int. Conf. on Development and Application Systems (DAS) (IEEE, 2024) pp. 87~90.
[4] S. Khan, T. Mazhar, T. Shahzad, A. Bibi, W. Ahmad, M. A. Khan, M. M. Saeed, and H. Hamam, Discover Sustainability **5**, 412 (2024).
[5] P. Sharma, R. N. Tiwari, P. Singh, P. Kumar, and B. K. Kanaujia, Sensors **22**, 7813 (2022).
[6] X. Zhang, C. Cao, and C. Song, IEEE Antennas Wireless Propag. Lett. **23**, 2728 (2024).
[7] S. A. M. Osman, M. S. El-Gendy, H. M. S. El-Hennawy, and E. A. Abdallah, Prog. Electromagn. Res. M **112**, 243 (2022).
[8] M. A. Sufian, N. Hussain, D. Choi, Y. Chun, Q. Hussain, and N. Kim, in Proc. 18th European Conf. on Antennas and Propagation (EuCAP) (IEEE, 2024) pp. 1~3.
[9] M. D. Ardakani, H. Tadayon, R. Karimian, S. Ahmadi, and M. Zaghloul, in Proc. 2023 IEEE Int. Symp. on Antennas and Propagation and USNC-URSI Radio Science Meeting (IEEE, 2023) pp. 709~710.
[10] U. Venkatesh, U. Subba Rao, and N. Sugitha, Int. J. Res. Sci. Technol. **12**, 33 (2025).
[11] T. Alahmad, M. Neményi, and A. Nyéki, Agronomy **13**, 2603 (2023).
[12] D. Araújo, C. Marques, H. Oliveira, and J. Piteira, in Proc. 2024 Smart Systems Integration Conf. and Exhibition (SSI) (IEEE, 2024) pp. 1-4.
[13] M. S. M. Rafi, M. Behjati, and A. S. Rafsanjani, arXiv: 2503.11162 (2025).
[14] R. Kumar, P. Bhardwaj, and M. Novita, in Proc. 2024 Int. Conf. on Computing, Sciences and Communications (ICCSC) (IEEE, 2024) pp. 1~5.
[15] C. A. Suárez Fajardo, M. A. González Jaramillo, C. A. Echeverry Moreno, and G. A. Puerto Leguizamón, Inge CuC **16**, 104 (2020).
[16] S. Khan, O. Khan, S. A. A. Shah, J. Nasir, B. T. Malik, S. Khan, and S. Koziel, IEEE Internet Things J. **12**, 22350 (2025).
[17] M. Farran, S. Boscolo, A. Locatelli, A.-D. Capobianco, M. Midrio, V. Ferrari, and D. Modotto, IET Microw. Antennas Propag. **11**, 1616 (2017).
[18] A. Darvazehban, S. Khaledian, O. Manoochehri, and M. A. Salari, Microw. Opt. Technol. Lett. **60**, 709 (2018).
[19] A. Prakash, N. Chattoraj, and S. B. Shukla, Microw. Opt. Technol. Lett. **60**, 725 (2018).
[20] Y. Al-Adhami and E. Ercelebi, Prog. Electromagn. Res. M **68**, 143 (2018).
[21] B. T. Ahmed, J. L. M. Campos, and D. B. Hernández, Microw. Opt. Technol. Lett. **61**, 1284 (2019).
[22] J. Geng, X. Liu, C. Liu, and H. Guo, Microw. Opt. Technol. Lett. **62**, 2569 (2020).
[23] J. Swathi, B. Jhansi, Y. S. Latha, P. Chaitanya, and C. Madhu, Int. Sci. J. Eng. Manag. **2**, (2023).
[24] E. V. J. Paays, S. Alam, and I. Sujati, J. Inform. Telecommun. Eng. **6**, 424 (2023).